Received: 10 February 2023 | Revised: 23 March 2023 | Accepted: 21 April 2023 | Published on: 10 May 2023

DOI: 10.1002/gamm.202300009

ORIGINAL PAPER

Continuation methods for lab experiments of nonlinear vibrations

Sebastian Tatzko | **Gleb Kleyman** | **Jörg Wallaschek**

Institute of Dynamics and Vibration Research, Leibniz University Hannover, Hannover, Germany

Correspondence
Sebastian Tatzko, Institute of Dynamics and Vibration Research, Leibniz University Hannover, Hannover, Germany. Email: tatzko@ids.uni-hannover.de

Funding information
German Research Foundation

Abstract

In this work, we will give an overview of our recent progress in experimental continuation. First, three different approaches are explained and compared which can be found in scientific papers on the topic. We then show S-Curve measurements of a Duffing oscillator experiment for which we derived optimal controller gains analytically. The derived formula for stabilizing PD-controller gains makes trial and error search for suitable values unnecessary. Since feedback control introduces higher harmonics in the driving signal, we consider a harmonization of the forcing signal. This harmonization is important to reduce shaker-structure interaction in the treatment of nonlinear frequency responses. Finally, the controlled nonlinear testing and harmonization is enhanced by a continuation algorithm adapted from numerical analysis and applied to a geometrically nonlinear beam test rig for which we measure the nonlinear forced response directly in the displacement-frequency plane.

KEYWORDS

control-based continuation, feedback control, force harmonization, nonlinear vibrations

1 | INTRODUCTION

Nonlinear vibration phenomena need to be well understood by engineers to assure safe operation. Therefore, experimental testing plays a key role in engineering design. Although simulative testing and virtual experiments are beneficial with respect to costs and reduced time to market, experiments on real structures are inevident for the final approval. Furthermore, intermediate testing could reveal design flaws and thus provide valuable feedback for product optimization. Nonlinearities can become a challenge, however, as vibration responses may be not unique and the jumping phenomenon as well as unstable regions exist. All these effects need to be tackled in the lab to get insight in the dynamics of the system.

By their nature, instabilities cannot be sustained in typical forced-response measurements. Additionally, free decay and hammer impact testing will yield obscured data caused by the frequency-energy dependence of the nonlinear vibration. For experimental characterization of nonlinear systems, Peeters et al. proposed force appropriation, also known as phase resonance testing, to investigate the resonance behavior [13,14]. They were able to extract the backbone curve from free decay after exciting the system to vibrate in an isolated nonlinear mode. In 2008, the idea of control-based continuation (CBC) was first presented by Sieber and Krauskopf [20]. They designed a feedback controlled experiment to analyze bifurcations of a parametrically excited pendulum. Barton and Burrow took the idea and applied CBC to an energy harvesting device with bistable response [3,5]. Different ways to implement the feedback control and the construction of frequency response curves have been proposed since. Basically, the idea of CBC is closely related to numerical

continuation, cp. [19], and Harmonic Balance [11]. A more efficient approach is proposed by Barton et al. [4] looking at so called S-curves at fixed frequency levels.

2 | DIFFERENT APPROACHES TO NONLINEAR FORCED RESPONSE MEASUREMENTS

In Figure 1 the frequency response to harmonic excitation of a Duffing oscillator is shown. The three-dimensional view reveals a characteristic manifold in the displacement-frequency-force space. We can now look at a slice for constant forcing level to get the typical nonlinear frequency response (NLFR) function for a hardening system. The displacement–frequency view is the one often looked at in numerical analyses with harmonic forcing. A not so common but interesting view is the displacement-force plot with so called S-curves. The name S-curve is derived from the shape seen in Figure 1D) which looks like the letter S at least in the Duffing case. A third approach is to consider the force-frequency relation at constant displacement which is known as *response-controlled stepped sine testing (RCT)* [8]. To build up the whole picture, one can choose to keep one parameter, displacement, force, or frequency, at a fixed level and measure the corresponding two dimensional curve given in Figure 1C–E. S-curves and RCT-curves can be easily assessed since they are unique for given displacement and given frequency, respectively. Barton et al. [4] proposed to stepwise increase the displacement level and use a fixed-point iteration to find the corresponding force in their controlled S-curve measurements. The constraint equations for eliminating higher harmonics of the force signal are written in form of a fixed-point problem and instead of applying Newton's method simple fixed-point iteration is used. Abeloos et al. [1] replaced the fixed-point iteration by adaptive FIR-filters for further reduction of measurement times. Similar to S-curves, Karaagacli and Özgüven [8,9] obtain the RCT-curve by stepping through the frequency values. For tracking

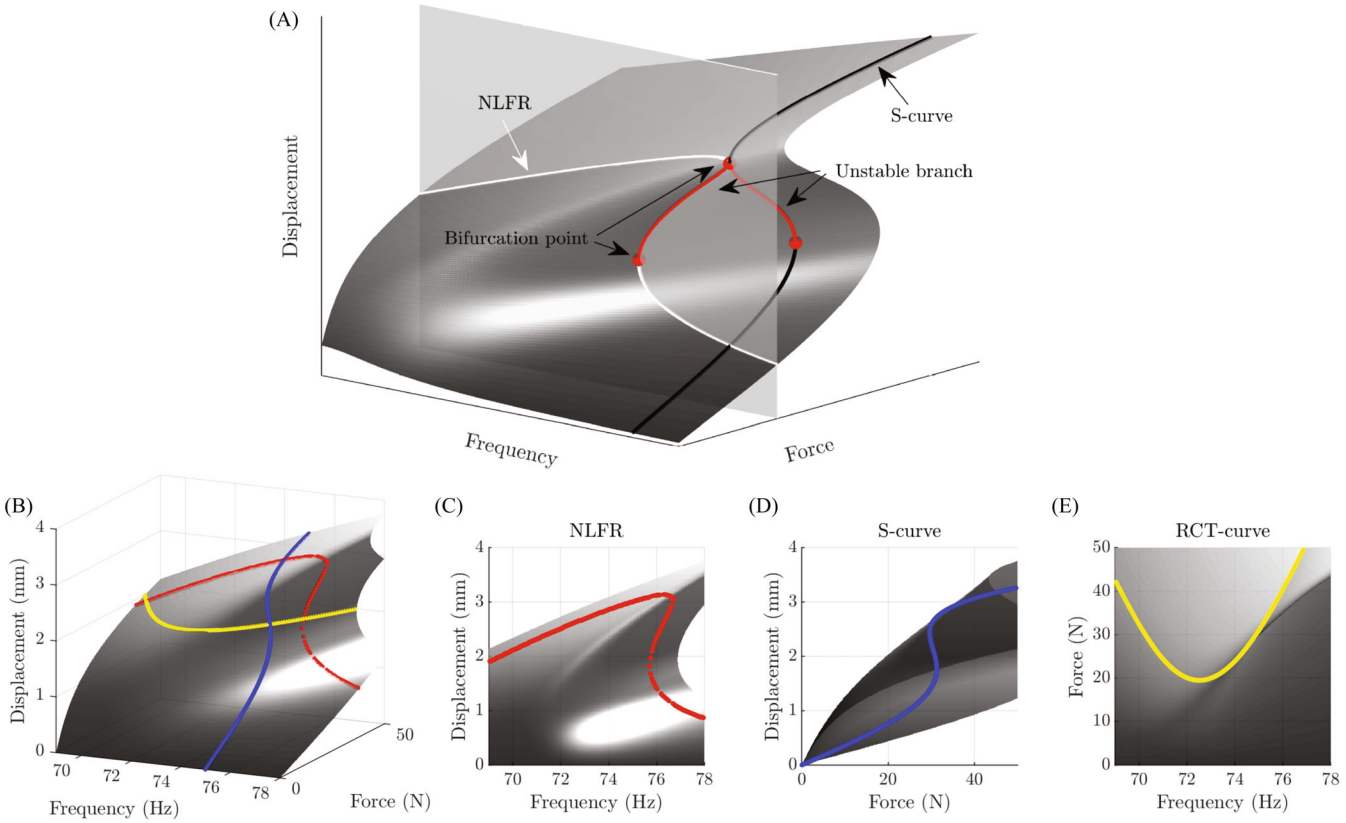

FIGURE 1 Different approaches to compute the nonlinear manifold of a Duffing oscillator: (A) Comparison of bifurcation points separating stable and unstable branches. (B) Three-dimensional view of different slices with typical curves resulting; (c) Nonlinear frequency response curve (NLFR) in the displacement-frequency plane; (d) S-curve in the displacement-force plane; (E) Response-controlled stepped sine testing curve (RCT) in the force-frequency plane.

NLFR-functions experimentally, a continuation algorithm with variable frequency is necessary comparable to numerical continuation. As the faster fixed-point iteration for S-curves is referred to as *simplified* method, see [16], we use the term *full* CBC for NLFR-continuation in the following.

Different approaches of CBC have been successfully used in nonlinear experiments so far. Renson et al. [15] realized a direct tracking of backbone curves, Kleyman et al. [10] analyzed steady-state vibrations of a structure with friction dampers, and Bureau et al. [6] were able to measure periodic response of an impact oscillator by applying stabilizing feedback control. In any case, a stabilizing feedback control is necessary to overcome instability of unstable branches of the response. The curves in Figure 1A exhibit regions where multiple response amplitudes exist for certain force and frequency values. Without feedback control these regions would not be accessible in the experiment. However, the feedback loop should not alter the dynamic system behavior which is referred to as *noninvasive control*, cp. [6]. In contrast to numerical analyses one needs to consider the closed loop setup and choose for suitable controller gains. While the feedback control changes the stability of the closed loop system, it is the stability of the open loop system that is actually of interest. Barton et al. [2] use an autoregressive moving average model on intentionally perturbed measurements to evaluate the actual stability. An alternative is proposed by Bureau et al. [7] who turn off the control for short period of time and observe the periodic orbit. Stability analysis in controlled nonlinear experiments is one of the current research topics in this field but will not be further addressed in this paper.

3 | FEEDBACK CONTROL AND CHOICE OF CONTROLLER GAINS

Figure 2 shows the closed loop setup where the actual nonlinear system under investigation is on the far right with input f_{exc} and output x. The actuator, for example, an electrodynamic shaker, is driven by a voltage signal u_{c} which is provided by a controller. The reference displacement x_{ref} may be computed from a continuation algorithm which is adapted from numerical analyses (full CBC) or from a fixed-point iteration (simplified CBC). For vibration control, a PD-controller is well suited and results in the following equation of motion for a Duffing oscillator

$$m\ddot{x} + d\dot{x} + kx + \alpha x^3 = f_{\mathrm{exc}}. \tag{1}$$

$$f_{\mathrm{exc}} = K_{\mathrm{p}}(x_{\mathrm{ref}} - x) + K_{\mathrm{d}}(\dot{x}_{\mathrm{ref}} - \dot{x}). \tag{2}$$

The excitation is replaced by the controller feedback and can now be set directly by the reference displacement and the reference velocity, respectively. Recasting the equation of motion of the closed loop system yields

$$m\ddot{x} + (d + K_{\mathrm{d}})\dot{x} + (k + K_{\mathrm{P}})x + \alpha x^3 = K_{\mathrm{p}}x_{\mathrm{ref}} + K_{\mathrm{d}}\dot{x}_{\mathrm{ref}}. \tag{3}$$

In Figure 3 the relation between output, reference and force amplitude is depicted assuming monoharmonic motion. Figure 3A shows that the PD-controller is able to bend the displacement-voltage relation. This results in modified $\hat{x}(\hat{x}_{\mathrm{ref}})$-curves shown exemplarily in Figure 3B for nonstabilizing and in Figure 3C for stabilizing controller gains. Note, that the S-curve projections displayed in the three-dimensional view (blue curves) are not affected by the feedback control. The PD-controller stabilizes the input-output relation which is the vibration amplitude $\hat{x}$ to a given reference signal $\hat{x}_{\mathrm{ref}}$. The force–displacement behavior can then be observed even on the branch which is unstable in open-loop configuration

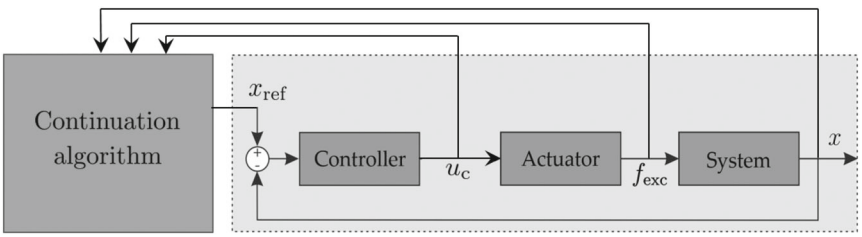

FIGURE 2 Scheme of the stabilizing feedback control building a closed loop with the actuator and the nonlinear dynamic system complemented by a continuation algorithm providing the reference signal x_{ref}.

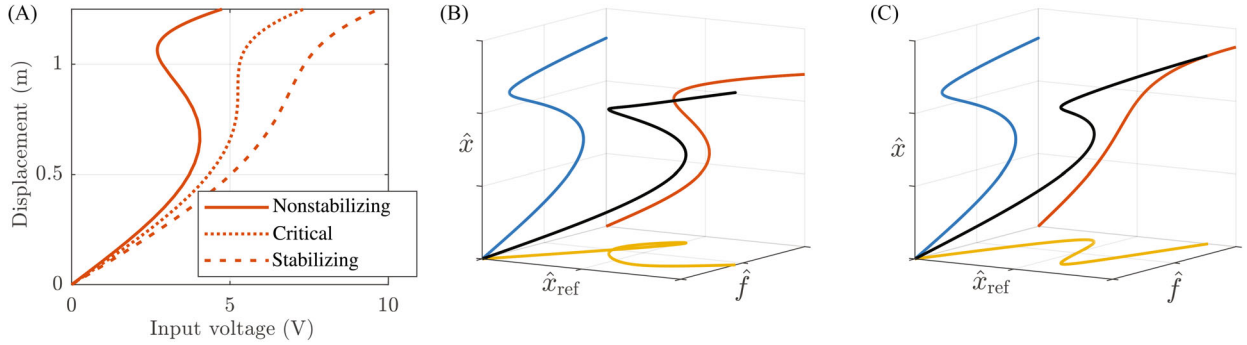

FIGURE 3 Stabilizing effect of feedback control: (A) Relation between voltage and displacement; (B,C) Relation of displacement, reference signal, and force for nonstabilizing (B) and stabilizing (C) feedback gains (colored curves are corresponding projections).

as shown below. Before getting into experimental results, the question on how to choose controller gains K_p and K_d will be addressed in the following analytical approach.

As we are interested in steady-state vibration response, harmonic motion is assumed to get an approximate solution as follows

$$x_{\mathrm{ref}} \approx \hat{x}_{\mathrm{ref}} \cos(\Omega t) = \frac{1}{2}\hat{x}\mathrm{e}^{\mathrm{i}\Omega t} + c.c., \tag{4}$$

$$x \approx \hat{x} \cos(\Omega t - \varphi) = \frac{1}{2}\hat{x}\mathrm{e}^{\mathrm{i}(\Omega t - \varphi)} + c.c., \tag{5}$$

where complex notation is used and *c.c.* denotes the complex conjugate of the given complex function. Inserting the complex harmonic functions in Equation (3) results in

$$\left((k + K_\mathrm{p}) - \Omega^2 m + \alpha\frac{3}{4}\hat{x}^2 + \mathrm{i}\Omega(d + K_\mathrm{d})\right)\hat{x}\mathrm{e}^{-\mathrm{i}\varphi} = \left(K_\mathrm{p} + \mathrm{i}\Omega K_\mathrm{d}\right)\hat{x}_{\mathrm{ref}}. \tag{6}$$

Here, the nonlinear Duffing term is approximated by its fundamental harmonic known as Harmonic Balance, cp. [21]. The reference amplitude can now be written as a function of the vibration amplitude in the form

$$\hat{x}_{\mathrm{ref}} = \hat{x}\frac{\sqrt{(k + K_\mathrm{p} - \Omega^2 m + \alpha\frac{3}{4}\hat{x}^2)^2 + \Omega^2(d + K_\mathrm{d})^2}}{\sqrt{K_\mathrm{p}^2 + \Omega^2 K_\mathrm{d}^2}}. \tag{7}$$

Stabilizing feedback control is defined by a unique relation between reference signal and output signal. The goal is to find controller gains which straighten this input–output behavior and enables unambiguous control by $\hat{x}_{\mathrm{ref}}$. Mathematically speaking, this control uniqueness is assured if Equation (7) has no extreme points, that is, no local maximum or minimum in the range of interest. From Equation (7) it is obvious that $\hat{x}_{\mathrm{ref}}$ is a cubic function for which two extreme points are possible. Thus, at the transition from a nonunique to a unique relation these extrema merge into a saddle point. To find this particular transition we compute the horizontal tangent for which we can use the derivative of the squared function

$$x_{\mathrm{ref}}^2 = \frac{\hat{x}^2}{K_\mathrm{p}^2 + \Omega^2 K_\mathrm{d}^2}\left(p_1^2 + p_1\alpha\frac{3}{2}\hat{x}^2 + \alpha^2\frac{9}{16}\hat{x}^4 + p_2^2\right). \tag{8}$$

$$p_1 = k + K_\mathrm{p} - \Omega^2 m. \tag{9}$$

$$p_2 = \Omega(d + K_\mathrm{d}). \tag{10}$$

Here, p_1 and p_2 are introduced to keep things clear. The derivative with respect to $\hat{x}$ then reads

$$\frac{\mathrm{d}\hat{x}_{\mathrm{ref}}^2}{\mathrm{d}\hat{x}} = \frac{2\hat{x}}{K_{\mathrm{p}}^2 + \Omega^2 K_{\mathrm{d}}^2}\left(p_1^2 + 3p_1\alpha\hat{x}^2 + \alpha^2\frac{27}{16}\hat{x}^4 + p_2^2\right) \stackrel{!}{=} 0. \tag{11}$$

For nontrivial solutions the term in brackets must vanish and we obtain a quartic equation with even exponents

$$\hat{x}^4 + \frac{16}{9\alpha}p_1\hat{x}^2 + \frac{16}{27\alpha^2}(p_1^2 + p_2^2) \stackrel{!}{=} 0. \tag{12}$$

This equation can be solved for $\hat{x}^2$ using the quadratic formula

$$\hat{x}^2 = -\frac{8}{9\alpha}p_1 \pm \sqrt{\left(\frac{8}{9\alpha}\right)^2 p_1^2 - \frac{16}{27\alpha^2}\left(p_1^2 + p_2^2\right)}. \tag{13}$$

As mentioned above, the transition to overcome ambiguous output happens for merging roots for which the square root in Equation (13) vanishes. From these considerations a coupling equation of the controller gains is obtained which reads

$$p_1^2 = 3p_2^2 \Leftrightarrow (k + K_{\mathrm{p}} - \Omega^2 m) = \pm\sqrt{3}\Omega(d + K_{\mathrm{d}}). \tag{14}$$

We are now able to provide a function of the minimum or critical value $K_{\mathrm{d,crit}}$ for a given proportional gain K_{p}

$$K_{\mathrm{d,crit}}(K_{\mathrm{p}}) = -\frac{1}{\sqrt{3}\Omega}(k + K_{\mathrm{p}} - \Omega^2 m) - d. \tag{15}$$

Surprisingly, the formula for calculating the critical controller gain dos not depend on the Duffing factor α. The stabilization criterion is only affected by the type of nonlinearity and not by its intensity. Hence, stabilizing gains can be found from linearized system parameters k, d, m, and the type of nonlinearity involved, which is cubic in this case. For nonlinearities other than cubic, the procedure described above needs to be adapted. Furthermore, in Equation (14) different signs need to be considered due to removing the square root. For the Duffing nonlinearity the frequency range with multiple possible response amplitudes is located above the natural frequency of the underlying linear system $\omega_0 = \sqrt{k/m}$, cp. Figure 1. Consequently, the feedback control is needed for excitation frequencies $\Omega > \omega_0$. It follows that only the negative sign is meaningful for the critical differential gain in Equation (15) from which positive values are obtained.

The derived formula for stabilizing controller gains is tested on a laboratory Duffing experiment shown in Figure 4A. A mass supported by guitar strings is harmonically forced by a voice coil actuator (VCA). The VCA is driven by a power amplifier for electrodynamic shakers by TIRA which was used in current-mode where the output current could be controlled directly. The motion of the mass is measured with a displacement sensor, and in parallel, a single-point laser vibrometer is used to determine its velocity. Thus, no derivation is required, which could affect the signal quality. The motion of the mass perpendicular to the strings results in a hardening oscillator which can be approximated by a single degree of freedom Duffing oscillator. Mass, stiffness, and damping parameters are obtained from experimental modal analysis at low vibration level and the nonlinearity is assumed to be pure cubic. System parameters are $m = 0.196$ kg, $d = 0.105$ Ns/m, $k = 693$ N/m.

Since the critical controller gain $K_{\mathrm{d,crit}}(K_{\mathrm{p}})$ also depends on the frequency Ω (cp. Equation 15) we chose S-curve measurement at fixed frequency steps for validation. However, the derived stabilizing controller gain formula is not restricted to one of the three approaches explained above (NLFR, S-curve, RCT-curve). Figure 4B shows resulting forced response functions of the nonlinear oscillator which are interpolated through several S-curves. The S-curves used are shown in Figure 4C. Figure 4D gives another view of the same plot to get a better picture of the spatial representation. Although the simplified CBC with stepwise increase of reference displacement values is fast, it takes a lot of data points to get one interpolated NLFR. A full CBC with advanced continuation directly in the displacement-frequency plane could be more efficient in some cases.

The S-curves shown in Figure 4 were successfully measured even on the branch which is unstable in open-loop configuration. We studied different controller gains and analyzed their influence on the S-curve measurement. In Figure 5A,B

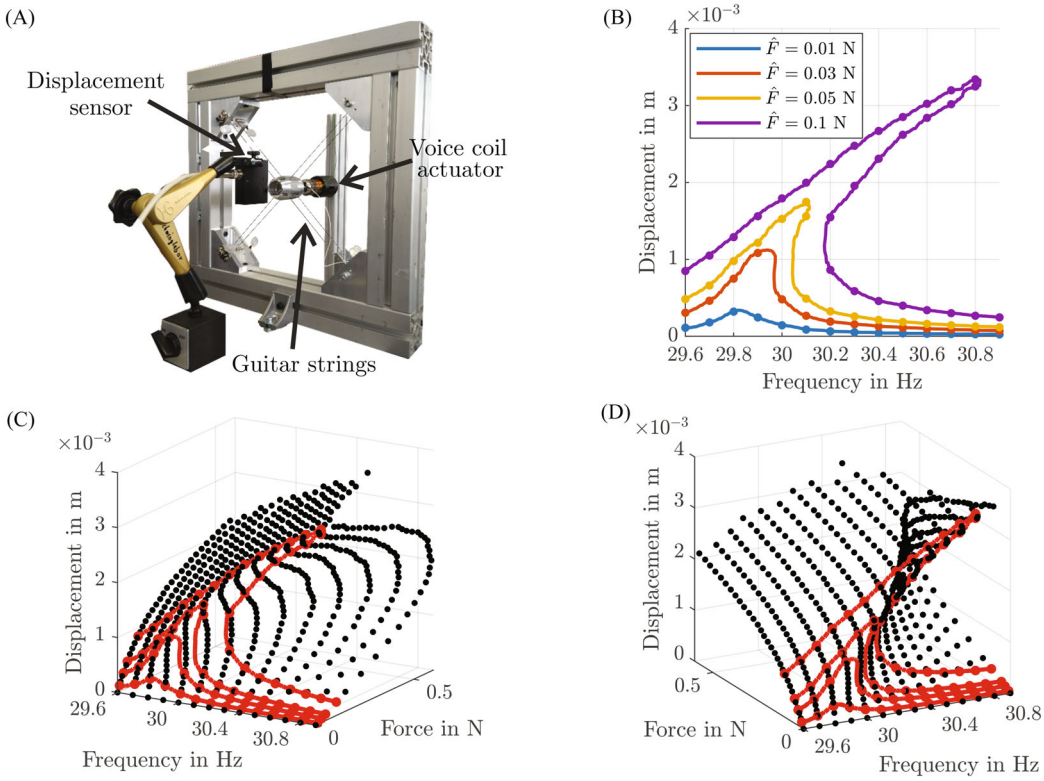

FIGURE 4 Experimental Duffing oscillator: (A) Test rig; (B) extracted frequency response curves; (C) S-curve measurement (black dots) with interpolated response curves (red); (D) another view of the measured S-curve manifold.

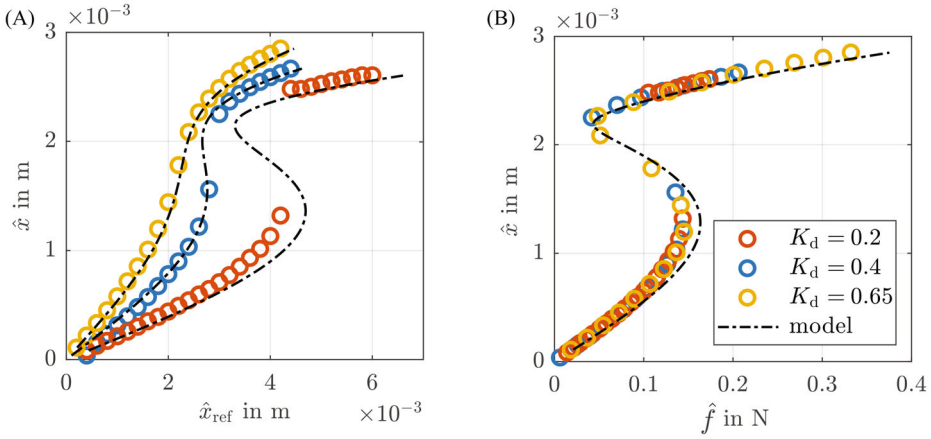

FIGURE 5 Measurement of the S-curve at 30.3 Hz for different values of K_{d} while $K_{\mathrm{p}} = 0$: (A) Relation between $\hat{x}_{\mathrm{ref}}$ and $\hat{x}$; (B) Corresponding S-curve.

the S-curve measurement at frequency 30.3 Hz is plotted where $K_{\mathrm{p}} = 0$ and values for K_{d} are varied. For $K_{\mathrm{d}} = 0.2$ no stabilizing effect is observed and a jump in the measurement from one stable branch to the other is the consequence. Above the critical value $K_{\mathrm{d,crit}} = 0.47$ the relation between $\hat{x}$ and $\hat{x}_{\mathrm{ref}}$ is unique and for $K_{\mathrm{d}} = 0.65$ a decent S-curve was identified, cp. Figure 5B. In Figure 6A the critical differential controller gain is plotted over the proportional controller gain K_{p} resulting in a straight line dividing stabilizing from nonstabilizing gain combinations. The critical value $K_{\mathrm{d,crit}} = 0.47$ for $K_{\mathrm{p}} = 0$ is found here since the results also belong to the S-curve measurement at 30.3 Hz. We chose a fixed value of $K_{\mathrm{d}} = 0.3$ to investigate the influence of the proportional gain. In Figure 6B–D the resulting S-curve measurements are plotted. For the nonstabilizing value (red circle) the S-curve is not completely accessible. A value that is well within the

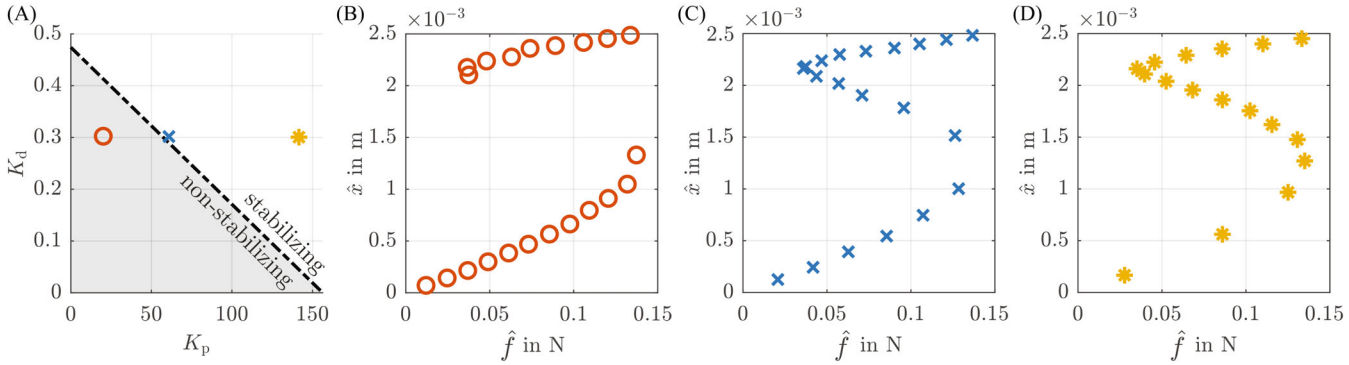

FIGURE 6 Variation of the proportional gain K_p: (A) $K_d - K_p$-plot with critical limit for stabilizing gains; (B–D) Measured S-curve data points corresponding to gain values marked in (A).

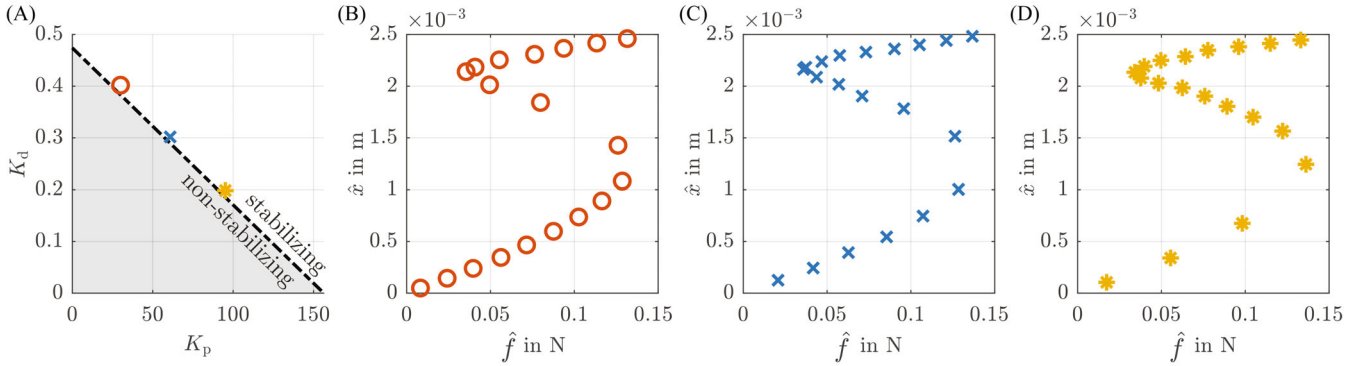

FIGURE 7 Variation of controller gains close to stabilizing limit line: (A) $K_d - K_p$-plot with critical limit for stabilizing gains; (B–D) Measured S-curve data points corresponding to gain values marked in (A).

stabilizing area (yellow asterisk) comes at the cost of reduced resolution on the lower branch, see Figure 6D, whereas a value closer to the stabilizing limit gives a fair distribution of measurement points along the curve (blue cross). Next, we investigated different gain combinations parallel to the stabilizing limit. In Figure 7A three pairs of K_d, K_p values are given. The blue cross is not changed but the other two combinations. Measurement results in Figure 7B–D reveal that the distribution of data points along the curve is affected by the choice of controller gains even though all gain pairs are able to stabilize the measurements. Note that the results presented here are obtained for a fixed stepsize of the reference signal $\hat{x}_{\text{ref}}$, cp. Figure 5A. One can certainly change the stepsize of the reference signal during measurement, but nevertheless it is advantageous to know about the influence of controller gains on data resolution. The here presented approach to systematically find stabilizing controller gains is an advantage over trial and error search for suitable values. Alternatively, Li and Dankowicz [12] proposed an adaptive control design which was tested on linear vibrations with uncertainty and can be used in CBC as well.

4 | HARMONIZATION OF THE EXCITATION SIGNAL

Taking a closer look at Figure 2 it becomes apparent that higher harmonics in the nonlinear vibration signal are fed back into the system unfiltered. For many systems that vibrate predominantly in their fundamental mode, this may not be much of a problem. However, nonlinear multi degree of freedom systems could be artificially internally excited when higher harmonics are close to other nonlinear modes. Moreover, Renson et al. [17] found that higher harmonics in the applied force signal can have significant, not yet explained, influence on the system stability. To avoid destabilizing or biased measurements a harmonization of the excitation is usually implemented along with control based continuation. For this purpose, the periodic signals are decomposed into their harmonic components. The voltage signal exemplarily

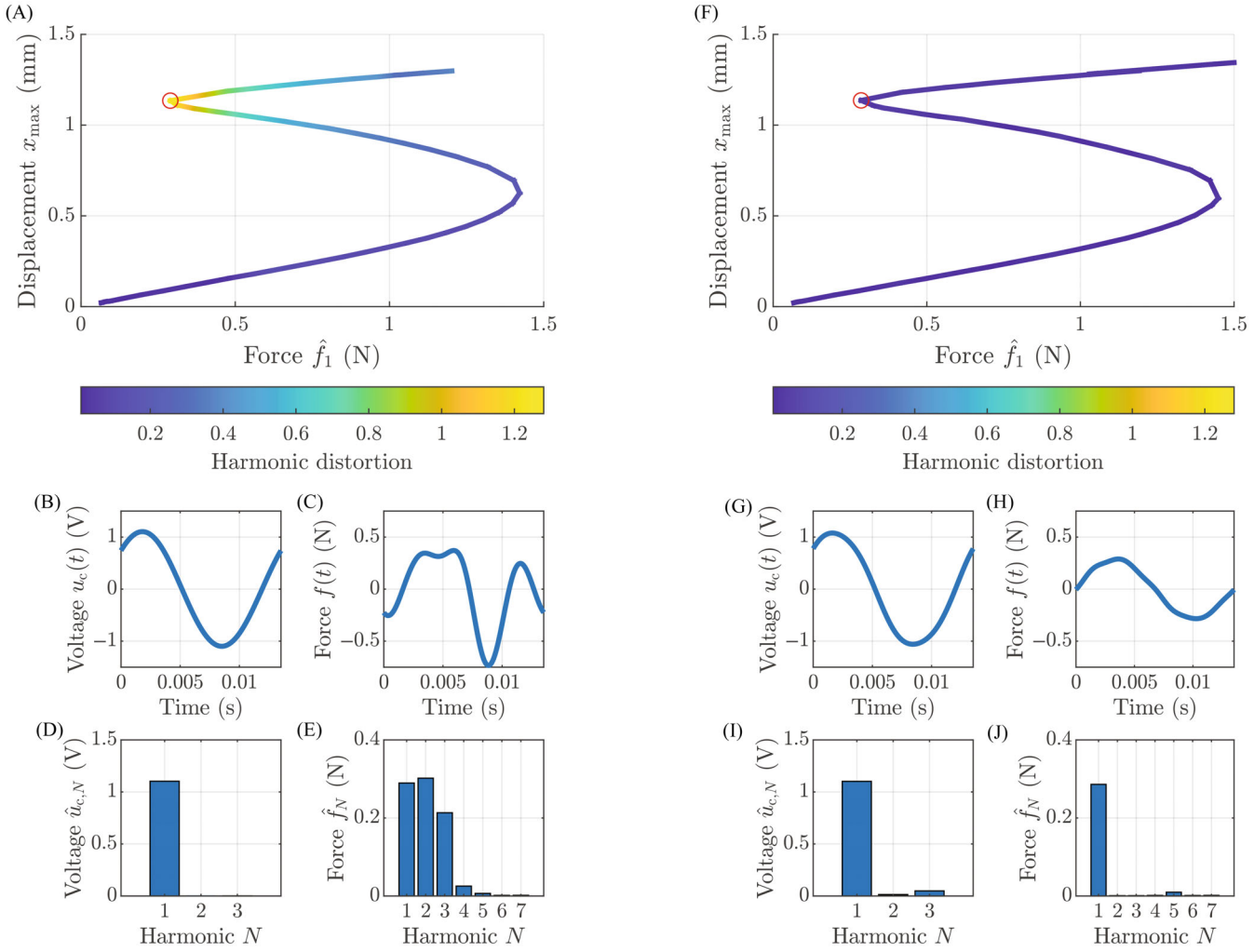

FIGURE 8 Analysis of harmonic distortion and signal harmonization: (A) S-curve with harmonized voltage signal; (B–E) Voltage and force signals along with representations of their harmonic content; (F) S-curve with harmonized force signal; (G–J) Voltage and force signals along with representations of their harmonic content.

reads

$$u_c(t) = \sum_{k=1}^{N} U_{k,s} \sin(k\Omega t) + U_{k,c} \cos(k\Omega t), \tag{16}$$

and other signals of displacement and force are decomposed accordingly. The Fourier spectrum is then limited to a certain amount of harmonics to approximate the generally periodic signals. In the simplified CBC a harmonization of the voltage signal u_c is typically used. However, we found that this approach leads to a non-negligible distortion of the forcing signal. In Figure 8A a S-curve measurement with harmonic distortion information is plotted obtained from the doubly clamped beam test rig described below, cp. Figure 9A. The maximum harmonic distortion is found at the red circled data point. Figure 8B–E shows the corresponding voltage and force signal and their harmonics, respectively. Second and third harmonic components are iterated out of the voltage signal to get a close to harmonic input to the electrodynamic shaker. There is however a clear shaker-structure interaction present leading to non-harmonic forcing into the dynamic system. We therefore focused on the forcing function itself and canceled out the harmonic components of second and third order in the force directly. Figure 8F shows the resulting S-curve with harmonic distortion information. There is a much lower level of distortion visible compared to the same plot on the left hand side. The resulting voltage signal required for the

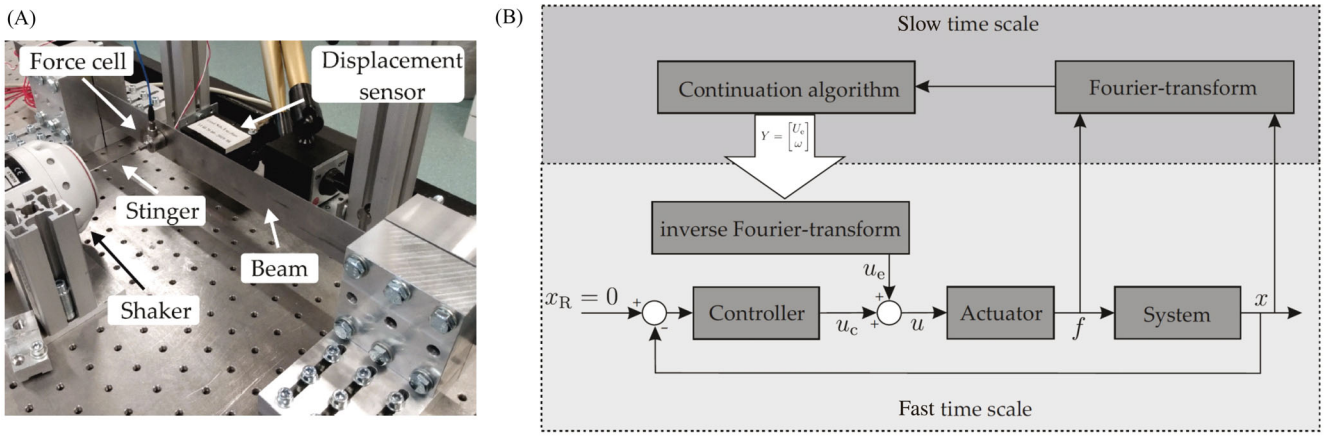

FIGURE 9 (A) Doubly clamped beam test rig with shaker and displacement sensor; (B) Scheme of full control-based continuation with stabilizing feedback control in the fast time scale and continuation based on Fourier coefficients in the slow time scale.

force harmonization is still quite harmonic with only little contribution of second and third harmonic terms, cp. Figure 8I. These little higher harmonic voltage components however are necessary to bring the forcing signal close to harmonic. The fifth component in Figure 8J is nonzero which is due to the fact that only the second and third components were canceled in the Newton procedure while the fourth component has no contribution here. Within the full CBC scheme presented in the following section, force harmonization is used in the NLFR-measurement to compensate unwanted excitation. In addition, the elimination of higher harmonics in the force signal can also be beneficial for S-curve and RCT analysis.

5 | EXPERIMENTAL CONTINUATION OF NLFR FUNCTIONS

The academic Duffing oscillator from Figure 4 is fairly insensitive with respect to exciter–structure interaction. In other words, the harmonic excitation signal is not notably distorted by the oscillation itself what indicates the applicability of the results for stabilizing controller gains for which harmonic motion is assumed. However, forced vibrations are typically investigated using electrodynamic shakers in the lab. A shaker may already show nonlinear behavior itself when displacement amplitudes at the driving point are large near resonances, cp. [23]. For the full CBC implementation we set up a nonlinear doubly clamped beam experiment, see Figure 9A. The beam is a thin steel structure (370 by 40 by 1.5 mm) clamped at both ends between solid aluminum blocks. An electrodynamic shaker is coupled to the beam structure via a stinger and a force sensor. In addition to the shown displacement sensor, a single-point laser vibrometer is also used for velocity measurement at the same point of the beam. The vibrometer is not shown in the figure. The clamped beam exhibits a hardening geometric nonlinearity that is caused by midplane stretching. When the beam is excited to vibrate in its first bending motion, the response to harmonic forcing can be described using the single-nonlinear-mode theory, cp. [22]. In a first approximation the equation of motion is that of a hardening Duffing oscillator which is why the nonlinear beam closely follows the previous results. From the above derived relation we know how the proportional and the differential gain affect the result. Based on an initial guess, the final gain values were chosen after educated adjustment considering the findings presented in Section 3. However, suitable controller gains for the entire instability region of the response curve remain a compromise due to Ω-dependence, so experience still plays an important role.

We are now interested in a universal implementation of CBC with predictor-corrector continuation for tracking arbitrary target functions. Figure 9B shows the extended CBC-scheme with the feedback control at the bottom to stabilize the unstable branches using a PD-controller. A simplified CBC with stepping through reference displacement signal could be used, but is set to zero here. Instead it proved useful to superimpose a voltage signal u_e on the feedback voltage. Analogue to numerical analyses, the experimental continuation procedure is formulated in terms of Fourier coefficients in the frequency domain. The periodic time signals are decomposed into their harmonics using Fast Fourier transform.

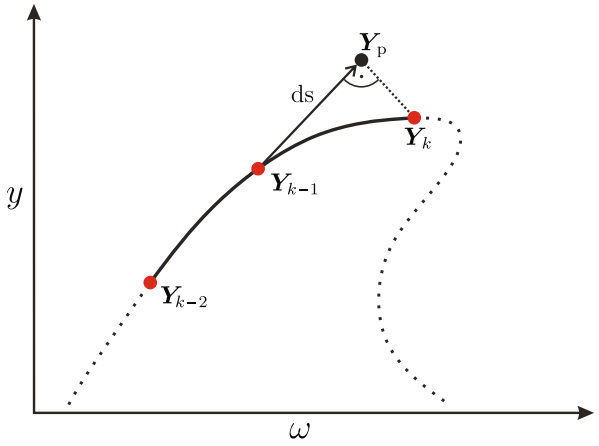

FIGURE 10 Illustration of the predictor-corrector continuation scheme used to implement the control-based continuation.

The solution vector then reads

$$\vec{Y} = \begin{bmatrix} U_{\mathrm{e,sin},1} \\ U_{\mathrm{e,cos},1} \\ \vdots \\ U_{\mathrm{e,sin},N} \\ U_{\mathrm{e,cos},N} \\ \Omega \end{bmatrix}. \tag{17}$$

Here, the excitation frequency Ω is part of the variables which is necessary to go back and forth in frequency direction at turning points. The next solution along the curve is obtained by a Newton-algorithm.

$$\vec{Y}_{i+1} = \vec{Y}_i - \mathbf{J}(\vec{Y}_i)^{-1}\vec{R}_i, \tag{18}$$

where $\mathbf{J}$ is the Jacobian and $\vec{R}$ is the residual function in which we define a certain fundamental harmonic forcing amplitude $F_{\mathrm{sin},1} = \hat{F}$

$$\vec{R} = \begin{bmatrix} F_{\mathrm{sin},1} - \hat{F} \\ F_{\mathrm{cos},1} \\ \vdots \\ F_{\mathrm{sin},N} \\ F_{\mathrm{cos},N} \\ r_{\mathrm{par}} \end{bmatrix}. \tag{19}$$

Any other harmonic coefficients of the force signal in the residual function will be minimized and eventually eliminated. The last entry in $\vec{R}$ is a constraint for continuation which is needed to balance the additional variable Ω in $\vec{Y}$ which defines how the curve is continued. The Jacobian needed to compute the next Newton iteration is calculated using a finite difference approach. Every parameter of $\vec{Y}$ is perturbed by a small value h which must not be too small to overcome measurement noise. If h is too large on the other hand the algorithm might converge away from the actual solution curve and jump to other minima. We use an adaptive perturbation step size which is calculated from the difference between the last two solution points

$$h_k = (Y_{k-2} - Y_{k-1})/2. \tag{20}$$

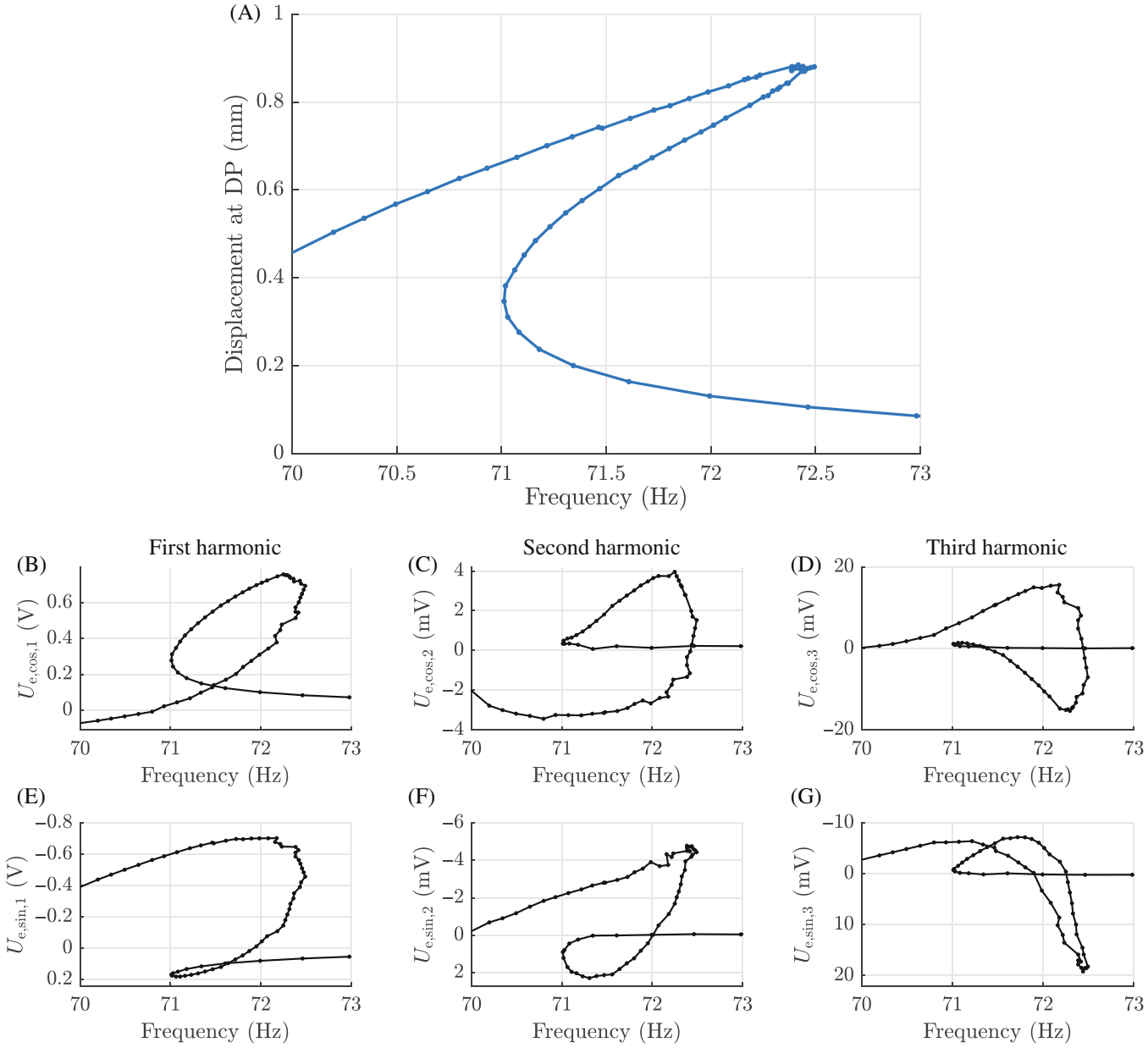

FIGURE 11 (A) Nonlinear frequency response curve from direct control-based continuation measurement; (B) Cosine component of the 1st harmonic; (c) Cosine component of the second harmonic; (D) Cosine component of the third harmonic; (E) Sine component of the 1st harmonic; (F) Sine component of the second harmonic; (G) Sine component of the third harmonic (note the different scaling of the y-axis for second and third harmonic)

The calculation of the full Jacobian can be very time consuming which is why a full update of the Jacobian is done only every fifth iteration. Between the full calculations only rank-one updates are performed, applying Broyden's method as proposed by Sieber and Krauskopf [20]. Schilder et al. [18] investigated how experimental continuation and Jacobian data can be improved when noise contamination plays a major role.

A next point on the branch is found by first going along the tangent from the last solution (tangent predictor). After that, the search direction is restricted to be orthogonal to the tangent (orthogonal corrector). This predictor-corrector approach is visualized in Figure 10. The mathematical expression for the orthogonal corrector reads

$$r_{\text{par}} = \left(\vec{Y}_{\text{p}} - \vec{Y}_{k-1}\right)^{\top} \left(\vec{Y}_{\text{p}} - \vec{Y}\right). \tag{21}$$

The full CBC continuation is implemented on a dSpace MicroLabBox which allows us execute Matlab/Simulink models in real-time. Furthermore, multiple input/output channels are available for communication between model and instrumentation. The sampling time of the MicroLabBox was set to 1/8000 s and the Fourier transform was performed with block length of 4000 samples. In order to reduce noise, three consecutive measurement repetitions were averaged before using the results in the continuation algorithm. Finally, a Hanning window was used to reduce leakage effects. The continuation problem was defined to have seven unknowns in the solution vector representing three harmonics (sine and cosine coefficients of each) plus the variable angular frequency Ω. Thus, second and third harmonic components have been canceled out of the force signal within this CBC test.

Figure 11A shows one NLFR solution curve measured with CBC directly in the given displacement-frequency plane. Additionally, subspaces of the harmonic components are plotted in Figure 11B–G. In each of the harmonic subspaces the solution path is in the shape of a helical loop revealing its contribution to the nonlinear resonance.

6 | CONCLUSIONS

In this paper, different approaches to implement control based continuation are discussed and applied to nonlinear experiments. With a focus on S-curve measurements, a general analytical formula for the choice of stabilizing feedback control gains is derived. This formula is set up for a Duffing type nonlinearity and helps to find suitable PD-controller gains which does not involve trial and error. An interesting finding is that stabilizing gains do not depend on the prefactor α of the Duffing nonlinear term but the qualitative nature of the nonlinearity alone. A feedback controller is then used to build up a predictor-corrector continuation to measure the NLFR function of a doubly clamped beam. We found that shaker–structure interaction needs to be addressed by eliminating the higher harmonics of the forcing directly. In some CBC experiments it is proposed to eliminate the higher harmonics of the voltage input to the shaker but that still produced nonharmonic forcing in our case. The continuation with feedback controller and force harmonization was eventually successful in NLFR measurement of the observed geometrically nonlinear beam.

AUTHOR CONTRIBUTIONS

Sebastian Tatzko: Conceptualization, Supervision, Methodology, Writing. **Gleb Kleyman**: Methodology, Writing, Editing. **Jörg Wallaschek**: Review, Editing.

ACKNOWLEDGEMENTS

The authors thank the German Research Foundation (DFG) for the support within the priority program SPP 1897 “Calm, Smooth and Smart.” Open Access funding enabled and organized by Projekt DEAL.

CONFLICT OF INTEREST

The authors declare no potential conflict of interests.

REFERENCES

[1] G. Abeloos, L. Renson, C. Collette, and G. Kerschen, Stepped and swept control-based continuation using adaptive filtering, Nonlinear Dyn **104** (2021), 3793–3808.
[2] D. Barton, Control-based continuation: Bifurcation and stability analysis for physical experiments, Mech. Syst. Signal Process. **84** (2017), no. Pt B, 54–64.
[3] D. A. W. Barton and S. G. Burrow, Numerical continuation in a physical experiment: investigation of a nonlinear energy harvester, J. Comput. Nonlinear Dyn. **6** (2010), no. 1, 011010.
[4] D. Barton and J. Sieber, Systematic experimental exploration of bifurcations with noninvasive control, Phys. Rev. E **87** (2013), 052916.
[5] D. Barton, B. Mann, and S. Burrow, Control-based continuation for investigating nonlinear experiments, J. Vibrat. Control **18** (2012), no. 4, 509–520.
[6] E. Bureau, F. Schilder, I. F. Santos, J. J. Thomsen, and J. Starke, Experimental bifurcation analysis of an impact oscillator – tuning a non-invasive control scheme, J. Sound Vibrat. **332** (2013), no. 22, 5883–5897.
[7] E. Bureau, F. Schilder, M. Elmegård, I. F. Santos, J. J. Thomsen, and J. Starke, Experimental bifurcation analysis of an impact oscillator–determining stability, J. Sound Vibrat. **333** (2014), 5464–5474.
[8] T. Karaağaçli and H. N. Özgüven, Experimental modal analysis of nonlinear systems by using response-controlled stepped-sine testing, Mech. Syst. Signal Process. **146** (2021), 107023.

[9] T. Karaağaçli and H. N. Özgüven, Experimental quantification and validation of modal properties of geometrically nonlinear structures by using response-controlled stepped-sine testing, Exp. Mech. **62** (2022), 199–211.
[10] G. Kleyman, M. Paehr, and S. Tatzko, Application of control-based-continuation for characterization of dynamic systems with stiffness and friction nonlinearities, Mech. Res. Commun. **106** (2020), 103520.
[11] M. Krack and J. Gross, *Harmonic balance for nonlinear vibration problems*, Springer Nature, Cham, Switzerland, 2019.
[12] Y. Li and H. Dankowicz, Adaptive control designs for control-based continuation in a class of uncertain discrete-time dynamical systems, J. Vibrat. Control **26** (2020), no. 21-22, 2092–2109.
[13] M. Peeters, G. Kerschen, and J. Golinval, Modal testing of nonlinear vibrating structures based on nonlinear normal modes: experimental demonstration, Mech. Syst. Signal Process. **25** (2011), 1227–1247.
[14] M. Peeters, G. Kerschen, and J. C. Golinval. *Modal testing of nonlinear vibrating structures based on a nonlinear extension of force appropriation* (22nd Biennial Conf. Mech. Vibrat. and Noise, Parts A and B, IDETC/CIE 1, 2009, 627–635.
[15] L. Renson, A. Gonzalez-Buelga, D. A. W. Barton, and S. A. Neild, Robust identification of backbone curves using control-based continuation, J. Sound Vibrat. **367** (2016), 145–158.
[16] L. Renson, D. Barton, and S. Neild, Experimental tracking of limit-point bifurcations and backbone curves using control-based continuation, Int. J. Bifurcat. Chaos **27** (2017), 1730002-1–1730002-19.
[17] L. Renson, A. D. Shaw, D. A. W. Barton, and S. A. Neild, Application of control-based continuation to a nonlinear structure with harmonically coupled modes, Mech. Syst. Signal Process. **120** (2019), 449–464.
[18] F. Schilder, E. Bureau, I. F. Santos, J. J. Thomsen, and J. Starke, Experimental bifurcation analysis–continuation for noise-contaminated zero problems, J. Sound Vibrat. **358** (2015), 251–266.
[19] R. Seydel, *Practical bifurcation and stability analysis*, Springer, New York, 2010.
[20] J. Sieber and B. Krauskopf, Control based bifurcation analysis for experiments, Nonlinear Dyn. **51** (2008), 365–377.
[21] S. Tatzko and M. Jahn, On the use of complex numbers in equations of nonlinear structural dynamics, Mech. Syst. Signal Process. **126** (2019), 626–635.
[22] J. J. Thomsen, *Vibrations and stability*, Springer, Berlin, 2003.
[23] G. Tomlinson, Force distortion in resonance testing of structures with electro-dynamic vibration exciters, J. Sound Vibrat. **63** (1979), 337–350.

How to cite this article: S. Tatzko, G. Kleyman, and J. Wallaschek, *Continuation methods for lab experiments of nonlinear vibrations*, GAMM-Mitteilungen. **46** (2023), e202300009. https://doi.org/10.1002/gamm.202300009